Mechanosensing and Sphingolipid-Docking Mediate Lipopeptide-Induced Immunity in *Arabidopsis*

Jelena Pršić[1†], Guillaume Gilliard[2†], Heba Ibrahim[3], Anthony Argüelles-Arias[1], Valeria Rondelli[4], Jean-Marc Crowet[2], Manon Genva[2], W. Patricio Luzuriaga-Loaiza[1], Estelle Deboever[2], M. Nail Nasir[2], Laurence Lins[2], Marion Mathelie-Guinlet[5], Sabine Eschrig[6], Stefanie Ranf[7], Stephan Dorey[8], Barbara De Coninck[3], Thorsten Nürnberger[9], Sébastien Mongrand[10], Monica Höfte[11], Cyril Zipfel[12], Yves F. Dufrêne[5], Magali Deleu[2T]*, and Marc Ongena[1T]*

[1]Microbial Processes and Interactions laboratory and [2]Laboratory of Molecular Biophysics at Interfaces, TERRA teaching and research centre, Gembloux Agro-Bio Tech, University of Liège, Gembloux, 5030, Belgium

[3]Division of Plant Biotechnics, Department of Biosystems, KU Leuven and KU Leuven Plant Institute, Heverlee, 3001, Belgium

[4]Department of Medical Biotechnologies and Translational Medicine, Università degli Studi di Milano, Segrate, 20090, Italy

[5]Institute of Biomolecular Science and Technology, Louvain University, Louvain-la-Neuve, 1348, Belgium

[6] Chair of Phytopathology, School of Life Sciences Weihenstephan, Technical University of Munich, Freising, 85354, Germany

[7]Department of Biology, Faculty of Science and Medicine, University of Fribourg, Fribourg, 1700, Switzerland

24 [8]Université de Reims Champagne Ardenne, RIBP-USC INRAE 1488, 51100 Reims , France

25 [9]Centre of Plant Molecular Biology, Eberhard-Karls-University Tübingen, Tübingen, 72076,
26 Germany

27 [10]Laboratoire de Biogenèse Membranaire, University of Bordeaux, Villenave d'Ornon, 33882,
28 France

29 [11]Laboratory of Phytopathology, Faculty of Bioscience engineering, Ghent University, Ghent,
30 9000, Belgium

31 [12]Department of Plant and Microbial Biology, Zurich-Basel Plant Science Center, University of
32 Zurich, Zurich, 8006, Switzerland

33

34 [†] JP and GG contributed equally to this article and share first authorship.

35

36 [τ] MD and MO contributed equally to the design and global supervision of the study and share
37 last authorship.

38

39 *Corresponding authors: M.D. (magali.deleu@uliege.be) and M.O. (marc.ongena@uliege.be)

40

Abstract

Bacteria-derived lipopeptides are immunogenic triggers of host defenses in metazoans and plants. Root-associated rhizobacteria produce cyclic lipopeptides that activate systemically induced resistance (IR) against microbial infection in various plants. How these molecules are perceived and give rise to IR remains elusive. Here, we reveal that immunity activation in *Arabidopsis thaliana* by the lipopeptide elicitor surfactin is mediated by docking into specific sphingolipid-enriched domains and relies on host membrane deformation and subsequent activation of mechanosensitive ion channels. This mechanism is distinct from host pattern recognition receptor-mediated immune activation and reminiscent of damage-induced plant immunity. It represents a novel aspect of plant immunization by mutualistic bacteria.

Main Text

Lipopeptides (LPs) represent a prominent and structurally heterogeneous class of molecules among the broad spectrum of small specialized metabolites synthesized by bacteria. Besides serving key functions for the ecological fitness of the producer (motility, biofilm formation, colonization, nutrient acquisition, or antagonism towards competing neighbors), some LPs also act as triggers of immune responses that restrict pathogen infection of metazoans and plants[1,2]. The vast majority of LPs formed by plant-associated bacteria are comprised of a partly or fully cyclized oligopeptide linked to a single fatty acid chain. Some of these cyclic lipopeptides (CLP) formed by beneficial species belonging to the *Pseudomonas* and *Bacillus* genera are potent elicitors of immune responses in the host plant leading to a systemically induced resistance (IR) against infection by microbial pathogens[2,3]. This CLP-induced plant resistance is a key process for biocontrol of crop diseases [4], but, in

65 contrast to pattern-triggered immunity (PTI), its molecular basis remains poorly understood.
66 Like in animals, PTI in plants relies on the detection of specific molecular motifs (Microbe-
67 Associated Molecular Patterns (MAMPs) via plasma membrane (PM)-localized Pattern-
68 Recognition Receptors (PRRs)[5]. Upon assembly of higher order receptor complexes involving
69 conserved co-receptors, PRRs activate receptor-like cytoplasmic kinases (RLCKs) such as BIK1
70 and its closest homolog PBL1 described as key convergent signaling hubs. This leads to
71 phosphorylation of numerous substrate proteins and subsequent induction of a well-
72 characterized immune response[6]. Early hallmarks of PTI signaling in plants include apoplastic
73 burst of reactive oxygen species ($[ROS]_{apo}$), calcium influx, medium alkalinization indicating
74 H^+/K^+ exchange and membrane depolarization, MAPK phosphorylation cascade and initiation
75 of transcriptional reprogramming [7,8,9,10].

76 The CLP surfactin (Srf, **Fig 1A**) is well conserved in plant beneficial bacilli[11] and is
77 among the bacterial compounds best described as immunity elicitor in several plant
78 species[2]. In *Arabidopsis thaliana* ecotype Col-0 (hereafter, *Arabidopsis*), root treatment with
79 purified Srf (at 10 µM as minimal active concentration previously determined[12] and used as a
80 mix of naturally produced homologues slightly differing in the length of the fatty acid tail,
81 see **Suppl Fig 1**) triggers IR and significantly reduces leaf infection by the grey mold pathogen
82 *Botrytis cinerea* (**Fig 1B**). Therefore, we used Srf as a model to further investigate the
83 molecular mechanisms determining CLP perception and immunity stimulation in *Arabidopsis*
84 root cells.

85 We first performed quantitative and time-resolved measurements of early responses
86 commonly associated with MAMP perception in *Arabidopsis* and other plants. $[ROS]_{apo}$ burst
87 is almost invariably associated with PTI[7] but, by contrast to treatment with the MAMP
88 flagellin-derived peptide flg22, we did not observe a $[ROS]_{apo}$ burst in *Arabidopsis* cells (roots

89 and leaves) treated with Srf based on a horseradish peroxidase-luminol assay (**Suppl Fig 2**).
90 Srf-mediated IR against *B. cinerea* is fully conserved in the *rbohD* mutant lacking functional
91 plasma membrane NADPH oxidase RBOHD responsible for MAMP-induced $[ROS]_{apo}$ burst[13]
92 (**Suppl Fig 3**). Hence, Srf-mediated activation of IR in the root does not require RBOHD[14].
93 However, Srf triggered a fast and consistent increase in intracellular ROS ($[ROS]_{intra}$) in root
94 loaded with the fluorescent probe DCFH-DA (**Fig 1C**). This Srf-triggered $[ROS]_{intra}$ burst is also
95 observed in the *rbohD* mutant (**Suppl Fig 4**), suggesting it is not caused by the uptake of
96 apoplastic ROS via aquaporins (as it is the case for the lower response to flg22, **Suppl Fig 5**)
97 but may originate from different organelles as reported for abiotic stresses or other small
98 microbial compounds[15,16,7,17]. Calcium influx typically associated with PTI in plants[8] was
99 tested upon elicitation by Srf using an aequorin-based bioluminescence assay. It did not
100 reveal any significant Ca^{2+} increase ($[Ca^{2+}]_{cyt}$) in root of the Col-0^{AEQ} reporter line in contrast
101 to the increase observed upon flg22 treatment (**Fig 1D**) or in response to chitin (**Suppl Fig 6**).
102 On the other hand, medium alkalinization occurs within minutes after Srf treatment (**Fig 1E**),
103 which indicates H^+/K^+ exchange possibly leading to membrane depolarization[9]. However, no
104 significant increase in conductivity was measured in the medium following Srf treatment
105 (**Suppl Fig 7**) indicating that the lipopeptide does not affect plasma membrane (PM) integrity
106 and does not cause massive electrolyte leakage. Cell viability tests confirmed that Srf is not
107 toxic for *Arabidopsis* root cells at concentrations up to 50 µM (**Suppl Fig 8**).

108 Next, we explored early changes in the root transcriptome profile induced within
109 hours by Srf via time course RNAseq analysis (30 min, 1h, 3h and 6h post treatment) using
110 the same setup previously reported for flg22 and the fungal MAMP chitin[18]. Data revealed a
111 relatively low transcriptional response to Srf elicitation over all sampling times with a total of
112 564 differentially expressed genes (DEGs, Log_2 Fold Change > 2, $p<0.05$; **Fig 1F**) compared to

113 approximately 5000 DEGs and 2000 DEGs reported upon flg22 and chitin treatment
114 respectively[18]. While MAMPs mainly up-regulate early responsive genes (30 min – 1 h)[18,19],
115 an almost equal number of up- and down-regulated DEGs were observed upon Srf treatment
116 at all time points (**Fig 1F**), with about half of the transcriptional changes specific to Srf
117 elicitation (47,9% and 58% compared with flg22 and chitin respectively)[18]. Strikingly, many of
118 the Srf down-regulated genes are upregulated by flg22 and chitin[18] (**Fig 1F, Suppl Table 1**).
119 Differential expression was confirmed by quantitative RT-PCR performed on some selected
120 genes in plantlets elicited with the lipopeptide and with chitin (**Suppl Fig 9**). Considering
121 DEGs involved in immune signaling and defense mechanisms, additional differences can be
122 observed between Srf and MAMP treatment. The expression of genes typically associated
123 with $[ROS]_{apo}$ burst such as *RBOHD(A)* are not modulated by Srf, unlike for flg22, while some
124 peroxidase genes are strongly upregulated and may be involved in ROS production and/or
125 homeostasis (**Fig 1G, Suppl Table 1**). We identified five down-regulated DEGs related to
126 calcium signaling but no genes linked to the MAPK phosphorylation cascade[10]. Within the
127 investigated time frame, Srf does not upregulate other common defense-related markers,
128 such as pathogenesis-related (PR) proteins or callose deposition, lignification genes and
129 receptor-like kinases (**Fig 1G**). Interestingly, *CYP71A12*, encoding a key enzyme of the
130 camalexin biosynthesis pathway[20], is among the late-responsive genes (6h) strongly
131 stimulated by Srf. In accordance, we measured significantly higher amounts of this
132 phytoalexin, which is toxic to *B. cinerea*[21,22], in infected leaves of Srf-treated plants
133 compared with controls (**Fig 1H**). The key role of camalexin in disease control was confirmed
134 by the loss of Srf-triggered resistance in the *pad3* mutant[23] unable to form camalexin[22] (**Fig**
135 **1I**). By contrast to PTI, which is associated with substantial transcriptional reprogramming[19],
136 immunity stimulation by Srf does not lead to major changes in the expression of genes

137 involved in signaling and defense.

138 Since the molecular basis of Srf-induced immune activation is signal-specific , we
139 hypothesized that plant cells perceive lipopeptides by a mechanism that differs from pattern
140 sensing. Srf possesses both a peptidic moiety and a fatty acid tail, but its IR-eliciting potential
141 is fully conserved in *Arabidopsis* mutants lacking functional PRRs that recognize either
142 bacterial proteinaceous immunogenic patterns or acyl chain epitopes such as medium chain
143 3-hydroxy fatty acids and HAAs[24,25] (**Suppl Fig 10**). Srf elicitation is also not significantly
144 affected in mutants lacking co-receptors required for proper functioning of a wider range of
145 PRRs detecting immunogenic peptides such as Pep1[26], nlp20[27] and IF1[28] nor in the *bik1 pbl1*
146 double mutant lacking RLCKs that act downstream of the PRR-co-receptor complexes (**Suppl**
147 **Fig 10**). Although we only tested a small subset of the multitude of PRRs potentially
148 expressed in *Arabidopsis*[6] and although early cellular signaling may be BIK1/PBL1-
149 independent[29], our data strongly suggest that *Arabidopsis* does not sense Srf via PRR-type
150 cell surface sentinels. This is in accordance with previous data from tobacco, which showed
151 that Srf is still active on protease-treated cells and that there is no refractory state upon
152 repeated Srf treatment unlike typically observed for PTI[30].

153 Due to their amphipathicity, CLPs readily interact with biological membranes, causing
154 pore formation and membrane disruption responsible for their antimicrobial activities[31].
155 Such an adverse effect is not expected on plant membranes, but we hypothesized that Srf
156 perception by root cells might primarily rely on its interaction with the lipid phase of the PM.
157 Complex sphingolipids glucosylceramides (GluCer) and glycosyl inositol phosphorylceramides
158 (GIPC) constitute more than 30% of *Arabidopsis* PM lipids and are key components required
159 for membrane integrity and functionality, notably by forming ordered nano-domains with
160 sterols[32,33,34]. *In silico* docking simulation first revealed a more favorable interaction of Srf

161 with GluCer or GIPCs than with the other typical plant PM lipids PLPC (1-Palmitoyl-2-
162 linoleoyl-sn-glycero-3-phosphocholine as phospholipid) and ß-sitosterol (as main sterol) (**Fig**
163 **2A**). To test this experimentally, we generated biomimetic liposomes using commercially
164 available GluCer, PLPC and ß-sitosterol. Isothermal titration calorimetry performed on
165 liposomes with increasing composition complexity in such lipids showed the highest binding
166 affinity of Srf to model membranes containing GluCer (**Fig 2B**). In support of a preferential
167 interaction with sphingolipids, molecular dynamic (MD) simulation on the same ternary lipid
168 system showed the specific insertion of Srf in the vicinity of GluCer molecules or in GluCer-
169 enriched areas in the membrane (**Fig 2C**). In light of these results, we tested Srf elicitor
170 activity on the *Arabidopsis* ceramide synthase mutant *loh1* (LONGEVITY ASSURANCE 1
171 HOMOLOG1) which is depleted in these complex sphingolipids[35,36]. We observed strongly
172 reduced $[ROS]_{intra}$ responses (**Fig 2D**) as well as loss of IR to *B. cinerea* infection in *loh1*
173 compared to wild-type plants (**Fig 2E**). Such lipid-dependent $[ROS]_{intra}$ elicitation was also
174 observed for other IR-eliciting CLPs such as orfamide and WLIP[2] isolated from beneficial
175 pseudomonads that resemble Srf in size and amphiphilic character (**Suppl Fig 11**). The CLP
176 immunogenic activity thus relies on an intricate interaction with PM sphingolipids as
177 reported for other microbial compounds[36,37,38].

178 By inserting into lipid bilayers, Srf may transiently affect the local structure of
179 membranes. Indeed, neutron reflectivity (NR) experiments (see **Suppl Fig 12** for deuterated
180 Srf synthesis and characterization) demonstrate that Srf exclusively inserts into the outer
181 leaflet of PLPC-ß-sitosterol-GluCer model membranes (**Fig 3A**). This is supported by MD
182 simulation showing that the Srf peptide backbone preferentially positions at the level of the
183 polar lipid heads of the membrane (**Suppl Fig 13**). Srf insertion does not affect the lipid
184 chain-chain interaction as shown by WAXS and FTIR (**Suppl Fig 13**). In addition, NR data

185 indicated that Srf insertion results in a decrease in membrane thickness (from 40 to 36Å),
186 which is more pronounced in ternary membranes than in membranes lacking GluCer (from
187 43 to 41Å) (**Suppl Table 4**). Analysis of the nanoscale morphology of supported PLPC-ß-
188 sitosterol-GluCer bilayers by Atomic Force Microscopy confirmed this membrane thinning
189 caused by Srf insertion (**Suppl Fig 14**). An additional impact of the lipopeptide on PM
190 physical properties derived from coarse-grained MD simulation which revealed a strong
191 curvature-inducing effect mediated by Srf docking on ternary membranes (**Fig 3B**).

192 In light of these biophysical data, a clear impact of Srf on PM structure can be
193 predicted but in integral root cells, the PM is physically connected to the thick and
194 mechanically strong cell wall polymer matrix, which provides structural support and might
195 stabilize the membrane into a flat conformation under low tension[39]. We thus next tested
196 early Srf-induced immune responses in cell wall-free protoplasts. Use of PPs renders the PM
197 more susceptible to deformation, which was used to study responses to cell swelling or
198 shrinkage/expansion during osmotic stresses[40,41]. As in root cells, Srf triggered a consistent
199 $[ROS]_{intra}$ burst in freshly isolated protoplasts (**Suppl Fig 15**). However, in contrast to roots, a
200 significant calcium influx, was observed in Srf-treated protoplasts by using the Col-0^{AEQ}
201 reporter line and also by loading Col-0 with the Fluo4-AM probe (**Fig3C and Suppl Fig 16**).
202 This Srf-induced Ca^{2+} influx is comparable in amplitude to the one induced by MAMPs (**Suppl**
203 **Fig 17**). It involves some PM channels since it is abolished in protoplasts pre-treated with the
204 general channel blocker $LaCl_3$ (**Suppl Fig 18**) and considering that the lipopeptide does not
205 cause any detrimental effect on protoplast viability at the concentration used (**Suppl Fig 19**).
206 Additional assays on protoplasts revealed that activation of early responses by Srf require
207 threshold concentrations of 5-10 µM both for calcium influx (**Fig 3D**) and $[ROS]_{intra}$ burst
208 (**Suppl Fig 20**), which is much higher than MAMPs detected at nanomolar concentrations.

209 This further indicates that Srf perception is not mediated by a high-affinity receptor-based
210 detection system and is in accordance with the mechanism predicted from biophysics in
211 which threshold amounts of Srf molecules must dock into sphingolipid domains in order to
212 modulate PM structure. We tested the impact of the lipopeptide on protoplast membrane
213 fluidity via measurements of laurdan generalized polarization (laurdan GP) related to the
214 lipid bilayer order. Our results show that Srf treatment led to a significant increase in ΔGP
215 values indicating a clear membrane rigidification effect as also observed upon interaction of
216 the lipopeptide with PM mimicking liposomes (**Fig 3E**).

217 Altogether, these data obtained with protoplasts support the relevance of PM
218 deformation in the response to Srf. We therefore hypothesized that insertion of the CLP
219 could induce physical constrains resulting in increased lateral tension sufficient for activating
220 mechano-sensitive (MS) ion channels, in a process similar to the one observed for some
221 anionic amphipathic chemicals[42,43]. This was supported by the reduced calcium influx
222 observed upon pre-treatment of Col-0^{AEQ} protoplasts with the specific MS channel blocker
223 GsMTX-4 (**Suppl Fig 21**). Among stretch sensitive mechanosensors identified so far in plant
224 cells, MSL9, MSL10 and MCA1/2 localize in the PM [44,45,46] but do not require RLCK-mediated
225 phosphorylation of the cytoplasmic domains for gating unlike other MS ion channels such as
226 OSCA1.3 which needs BIK1 phosphorylation to be activated [47]. Using Fluo-4, we thus tested
227 protoplasts prepared from the quintuple *msl4/5/6/9/10*[48] and the double *mca1/2*[49] mutants
228 for their response to Srf and observed a significantly decreased calcium influx, to the same
229 extent as chemical inactivation with GsMTX-4 in Col-0 (**Fig 3F**).

230 We next evaluated the effect of inactivation or knock-out of *msl* and *mca* channels on
231 intracellular ROS burst as early response of root tissues elicited by Srf. Pre-treatment with
232 GsMTX-4, $LaCl_3$ or with the Ca^{2+} chelator EGTA eliminated the ROS burst triggered by Srf in

233 root tissues (**Fig 3G**), supporting the importance of MS channels in the response and
234 indicating that ion fluxes acts upstream of or are interdependent of $[ROS]_{intra}$[8]. An almost
235 complete loss of $[ROS]_{intra}$ burst was also observed upon Srf treatment in the *msl4/5/6/9/10*
236 and *mca1/2* mutants as compared to Col-0 (**Fig 3H**). In addition, *mca1/2* and *msl4/5/6/9/10*
237 plants were strongly impaired in mounting systemic resistance against *B. cinerea* upon Srf
238 treatment (**Fig 3I**), further indicating that functional MS channels are necessary for full
239 response of *Arabidopsis* to Srf elicitation on roots. Data on protoplasts show that Srf may
240 trigger some calcium transients as early immune-related event but a detectable Ca^{2+} influx is
241 not required for defense activation in plantlets, which correlates with the fact that no
242 downstream components of calcium signaling are up-regulated upon perception of the
243 lipopeptide.

244 Collectively, although contributions of other channels cannot be ruled out[47], our data
245 provides evidence for a key role of PM-located mechanosensors in lipopeptide-induced plant
246 defenses. The relative contribution of each channel remains to be determined as they
247 display specific properties in terms of sensitivity to membrane tension and ion selectivity.
248 MCA1/2 are described as genuine transporters of Ca^{2+} [46,50] while MSL10 is regarded as a non-
249 selective ion transporter that is indirectly involved in calcium signaling upon wounding[51] and
250 response to hypo-osmotic shock in cell swelling[41]. Both channels may thus act in a
251 coordinated fashion to tailor ion fluxes leading to cellular responses and PM depolarization.
252 As previously reported for other plant species[2], treatment with Srf prepares *Arabidopsis* to
253 mount defense responses culminating in the systemically expressed IR phenotype. We
254 provide new insights into the molecular basis of the well-known long-standing process of
255 CLP-triggered plant immunity activation by unveiling a new lipid-mediated mechanism for
256 the detection of these molecules at the cell surface. We infer from our data that CLP

257 insertion into sphingolipid-enriched PM domains causes deformation and increases lateral
258 tension in the membrane leading to rearrangement of the MS protein complexes and gating
259 of the channels. This allows ion influx and initiates chemical signaling that can be integrated
260 by root cells to activate early immune responses in a process that remains to be deciphered.
261 Such a lipid-dependent perception at the cell surface may apply also to other bacterial
262 amphiphilic IR elicitors such as acyl-homoserine lactones and rhamnolipids which also
263 readily interact with membrane lipids and may thus be perceived via similar
264 mechanisms[2,52,53,54,55]. The nature of PM lipids widely varies across plant species[34]. This could
265 explain, at least in the case of Srf, why this molecule triggers immunity in dicots but is not
266 very active on monocots[2]. We assume that the effect of a CLP on a particular target
267 membrane is also fine-tuned by precise structural traits in the molecule. It may explain why
268 some CLPs produced by *Pseudomonas* leaf pathogens act as virulence factors in a wide range
269 of plants by causing necrosis via pore formation in cellular membranes[56]. However, further
270 investigation is required to capture the physico-chemical rules governing lipid selectivity and
271 CLP insertion dynamics. Clearly, this process differs from the receptor-based surveillance
272 system involved in the recognition of MAMPs by plant cells or in the perception of the
273 Pam_3CSK_4 analog of triacylated lipopeptides produced by *Staphylococcus aureus* and acting
274 as agonists of Toll Like-type PRRs in metazoans[57]. It therefore reflects a new aspect of plant-
275 microbe communication mediated by small chemicals from beneficial bacteria. Collectively,
276 our data show that Srf perception leads to specific immune activation signature regarding
277 the type, timing, and amplitude of early defense-related events and the weak transcriptional
278 reprogramming as compared to PTI. This may explain why elicitation by Srf is cost-effective
279 for the host plant as it does not result in growth-defense trade-off[58,59] nor does it cause a
280 strong response associated with the alertness state or a hypersensitive reaction leading to

281 cell death. Using CLPs as elicitors would enable bacteria to bypass a strong immune response
282 and avoid its rejection as undesirable associate. Further investigations are needed for a
283 comprehensive understanding of the whole process from perception to systemic signaling
284 leading to CLP-induced plant resistance. While this is challenging, it is mandatory to
285 rationally implement the use of these compounds or their producers as bio-sourced
286 alternatives to plant-protective chemicals in sustainable agriculture.
287

288 **Fig. 1. Surfactin triggers systemic resistance in *Arabidopsis* associated with atypical**
289 **immune responses. (A)** Structural model of the heptapeptide Srf (C14 acyl chain homologue)
290 in water (Gromacs v.4.5.4). Red: oxygen, white: hydrogen, dark blue: nitrogen, light blue:
291 carbon. The polar amino acids are circled in yellow, and other amino acids and the acyl chain
292 constitute the non-polar part of the molecule. **(B)** Disease incidence caused by *Botrytis*
293 *cinerea* in *Arabidopsis* Col-0 plants pre-treated with Srf (10 μM) or not (mock treatment, 0.1
294 % ethanol) (n=28 replicates from three independent experiments). The box plots encompass
295 the 1st and 3rd quartiles, the horizontal line indicates the median, and bars extend from the
296 lower to the higher values. Disease reduction (D.R.) is calculated from the mean values of
297 both treatments. Significant difference ***P<0.001, two-tailed t-test. **(C)** Burst in
298 intracellular ROS species in *Arabidopsis* Col-0 roots upon treatment with Srf (10 μM). Left,
299 time course of $[ROS]_{intra}$ accumulation (Relative Fluorescence Units, RFU) with data at each
300 time point representing mean ± SD, n=3 (independent root samples). Right, fold increase in
301 fluorescence values ± SD, at 30 min after the addition of Srf compared to mock-treated
302 roots. Data are pooled from three independent experiments (total n=9) and asterisks
303 indicate significant difference (***P<0.001, two-tailed t-test). **(D)** $[Ca^{2+}]_{cyt}$ kinetics in Srf-
304 treated (10 μM) or flg22-treated root tissues (1 μM) (n=6) compared to mock treatment in
305 the *Arabidopsis* Col-0^{AEQ} reporter line. Results are represented as luminescence counts per
306 second relative to total luminescence counts remaining (L/Lmax; mean ± SD). Experiments
307 were repeated three times with similar results. **(E)** pH variation in Col-0 root medium
308 following mock treatment or addition of 10 μM Srf. Values on the graph are normalized to
309 pH of the first time point ± SD and are from one representative experiment (n=4) out of 2
310 independent experiments showing similar results. **(F)** Number of DEGs (Log_2 Fold Change > 2,
311 P<0.05) in *Arabidopsis* root cells determined via RNAseq for each time point in response to

312 Srf treatment (10 μM). Our data were compared with those reported for DEGs in response
313 to flg22 (1 μM) and chitin (Chi, 1 mg/ml)[18] and bars are subdivided by the number of genes
314 specifically responding to Srf and by the number of genes differentially (oppositely)
315 regulated by Srf and the two MAMPs. **(G)** Heatmap of the expression of genes putatively
316 associated with plant immune responses (listed in Supp table 1) that were modulated upon
317 Srf treatment (S, left) (10 μM) and compared with their expression in response to flg22 (1
318 μM) and chitin (1 mg/ml) (F and C respectively, right) based on published data[18]. Colour
319 scale represents Log_2 FC (> 2, P<0.05). **(H)** Camalexin response associated with IR triggered
320 by Srf. Camalexin accumulation 96 hours post *B. cinerea* inoculation (hpi) in *Arabidopsis* Col-
321 0 leaves of mock- or 10 μM Srf-treated plants at the root level. Graph shows values obtained
322 in one experiment with each value representing a sample of five plants pooled together.
323 Asterisks indicate significant difference with ns, not significant; **P*<0.05; ****P*<0.001; two-
324 tailed *t*-test. **(I)** Disease incidence of *B. cinerea* in *pad3* mutant pretreated with 10 μM Srf or
325 mock-treated at the root level (n=30, values obtained from three independent experiments,
326 presented as differently shaded grey values). Data are represented as in fig 1B. Asterisks
327 indicate significant difference with ns, not significant; **P*<0.05; ****P*<0.001; two-way ANOVA
328 and Sidak's multiple-comparison post-test.
329
330 **Fig. 2. Affinity for sphingolipids determines CLP-triggered immunity. (A)** *In silico* docking
331 simulation of the interaction between Srf and plant PM lipids with their associated energy of
332 interaction (E_{int}). A lower E_{int} value indicates a more favorable interaction. Hydrogen, oxygen
333 and phosphate atoms are respectively represented in grey, red and blue. Carbon atoms of
334 Srf are in yellow and carbon atoms of GluCer, Sito and PLPC are in pink. **(B)** Binding
335 coefficient (K) of Srf to liposomes with different lipid compositions. Graph presents values

336 from two independent experiments, mean ± SD. **(C)** Molecular dynamics simulation of Srf
337 insertion in GluCer-enriched domains of a PLPC-Sito-GluCer bilayer. Left: Top views of
338 bilayers before and after Srf insertion (right). **(D)** $[ROS]_{intra}$ accumulation in roots of Col-0 and
339 *loh1* mutant. Data represents fold increase in fluorescence values ± SD (n=6 from two
340 independent experiments) at 30 min after Srf addition (10 μM) or not . Significant difference
341 ***P<0.001, two-tailed *t*-test. **(E)** Disease incidence of *B. cinerea* in *Arabidopsis* Col-0 and
342 *loh1* mutant plants, pre-treated with Srf (10 μM) compared with mock treatment (n=30 from
343 two independent experiments). Data are represented as in fig 1B. ns = not significant,
344 ***P<0.001, two-way ANOVA and Sidak's multiple-comparison post-test.

345 **Fig. 3. Srf causes membrane deformation and activates mechanosensitive channel-**
346 **dependent immune responses. (A)** Membrane thickness determined via neutron scattering
347 length density (SLD) profiles of supported PLPC-Sito-GluCer membrane before (black) and
348 after (green) Srf addition to the final 95:5 membrane: Srf molar proportion (0.24 μM)
349 (below). Illustration (above) presents the correspondence between regions in the SLD profile
350 and specific zones in the membrane. **(B)** Molecular dynamics simulation of Srf-induced
351 membrane curvature. **(C)** Left, $[Ca^{2+}]_{cyt}$ kinetics in Srf-treated (10 μM) root cell protoplasts
352 (n=6) compared to mock treatment in the *Arabidopsis* Col-0^{AEQ} reporter line. Results are
353 represented as luminescence counts per second relative to total luminescence counts
354 remaining (L/Lmax; mean ± SD). Experiments were repeated three times with similar results
355 (see Suppl Fig 16 for additional experiments). Right, increase in $[Ca^{2+}]_{cyt}$ detected upon
356 loading root protoplasts of Col-0 with Fluo-4 in mock- or Srf-treated (10 μM). Experiments
357 were repeated three times with similar results. **(D)** Dose-dependent $[Ca^{2+}]_{cyt}$ increase
358 induced by Srf in root protoplasts of *Arabidopsis* Col-0^{AEQ}. Values are the average of L/Lmax
359 values from 1.5 to 4 min after treatment corresponding to the top of the peak. Mean ± SD of

360 at least 10 technical replicates from at least five independent experiments. Asterisks indicate
361 statistically significant differences to the mock treatment (ns= no significant difference;
362 *P<0.05; ***P < 0.001; (a) two-tailed t-test; (b) Welch and Brown-Forsythe ANOVA). **(E)**
363 Change of laurdan generalized polarization (ΔGP) in Srf-treated (10 μM) Col-0 root
364 protoplasts and in liposomes reflecting a change of membrane rigidity. ΔGP is defined as the
365 subtraction of GP measured at 10 min following treatment and GP measured before
366 treatment. Mean ± SD of 12 (for protoplasts) and 15 (for liposomes) replicates from 8 (for
367 protoplasts) and 5 (for liposomes) independent experiments. ***P<0.001, two-way ANOVA
368 and Sidak's multiple comparison test. **(F)** $[Ca^{2+}]_{cyt}$ response measured with Fluo-4 upon Srf
369 elicitation (10 μM) in *Arabidopsis* Col-0 root protoplasts with and without pre-treatment
370 with the mechanosensitive channel blocker GsMTX-4 (10 min incubation, 7.5 μM)(n=10) and
371 in root protoplasts of the *mca1/2*, and *msl4/5/6/9/10* mutants (n=14). Mean ± SD from four
372 independent experiments. Letters represent statistically different groups at α = 0.05 (two-
373 way ANOVA and Tukey's multiple-comparison post-test). **(G)** $[ROS]_{intra}$ accumulation upon
374 addition of 10 μM Srf to *Arabidopsis* Col-0 roots upon pre-treatment or not (Col-0, n=16)
375 with the mechanosensitive channel blocker GsMTX-4 (10 min incubation, 7.5 μM) (n=12),
376 with the non-selective Ca^{2+} channel blocker $LaCl_3$ (10 mM) (n=7) and the Ca^{2+} chelator EGTA
377 (1 mM) (n=7). Data represent fold increase in fluorescence values 30 min after Srf addition
378 compared to mock-treated roots. Mean ± SD calculated from data from two independent
379 experiments. Letters represent statistically different groups at α = 0.05 (two-way ANOVA
380 and Tukey's multiple-comparison post-test). **(H)** $[ROS]_{intra}$ accumulation in *Arabidopsis* Col-0
381 (n=6), *mca1/2* (n=7), and *msl4/5/6/9/10* (n=8) roots following Srf treatment (10 μM). Data
382 represent fold increase in fluorescence values 30 min after Srf addition compared to mock-
383 treated roots. Mean ± SD from two independent experiments. **P<0.01, two-tailed t-test. **(I)**

384 Disease incidence of *B. cinerea* in *Arabidopsis* Col-0, *mca1/2*, and *msl4/5/6/9/10* mutant
385 plants, mock- or Srf pre-treated (10 μM)(each n=30 from two independent experiments
386 represented as differently shaded grey values). Data are represented as in fig 1B.

387

388 **Acknowledgments**

389 We thank Aurélien Legras, Sébastien Steels, Catherine Helmus, and Adiilah Mamode-Cassim
390 for their excellent technical support.

391

392 **Funding**

393 This work was supported by the EU Interreg V France-Wallonie-Vlaanderen portfolio
394 SmartBiocontrol (Bioscreen and Bioprotect projects, avec le soutien du Fonds européen de
395 développement régional - Met steun van het Europees Fonds voor Regionale Ontwikkeling),
396 by the European Union Horizon 2020 research and innovation program under grant
397 agreement No. 731077, by the PDR surfasymm (T.0063.19) from F.R.S.-FNRS (National Funds
398 for Scientific Research in Belgium) and by the EOS project ID 30650620 from the FWO/F.R.S.-
399 FNRS. G.G. is recipient of a F.R.I.A. fellowship (F.R.S.-FNRS), M.D. and M.O. are respectively
400 senior research associate and research director at the F.R.S.-FNRS.

401

402 **Author contributions**

403 J.P., G.G., M.D. and M.O. conceived and designed experiments; J.P., G.G., H.I., A.A., V.R.,
404 W.P.L-L, E.D., M.N.N., M.M-G., S.E. and Y.F.D. performed experiments and analyzed data; J-
405 M.C., M.G. and L.L. performed modeling; S.D., B.D.C, S.R., T.N., S.R., M.H. and C.Z.

406 substantially revised the manuscript and were involved in the discussion of the work; M.D.
407 and M.O. supervised the study and provided funding.
408
409 **Competing interests:** The authors declare no competing interests.
410
411 **References**
412

413 1. Mohammad, M. *et al.* Staphylococcus aureus lipoproteins in infectious diseases.
414 *Front. Microbiol.* **13**, 1–17 (2022).
415 2. Pršić, J. & Ongena, M. Elicitors of Plant Immunity Triggered by Beneficial Bacteria.
416 *Front. Plant Sci.* **11**, 1–12 (2020).
417 3. Cesa-Luna, C. *et al.* Charting the Lipopeptidome of Nonpathogenic Pseudomonas.
418 *mSystems* **8**, (2023).
419 4. Blake, C., Christensen, M. N. & Kovacs, A. T. Molecular aspects of plant growth
420 promotion and protection by bacillus subtilis. *Mol. Plant-Microbe Interact.* **34**, 15–25
421 (2021).
422 5. Zhang, L., Hua, C., Janocha, D., Fliegmann, J. & Nürnberger, T. ScienceDirect Plant
423 Biology into function and evolution. *Curr. Opin. Plant Biol.* **74**, 102384 (2023).
424 6. DeFalco, T. A. & Zipfel, C. Molecular mechanisms of early plant pattern-triggered
425 immune signaling. *Mol. Cell* **81**, 3449–3467 (2021).
426 7. Waszczak, C., Carmody, M. & Kangasjärvi, J. Reactive Oxygen Species in Plant
427 Signaling. *Annu. Rev. Plant Biol.* **69**, 1–28 (2018).
428 8. Köster, P., DeFalco, T. A. & Zipfel, C. Ca 2+ signals in plant immunity . *EMBO J.* **41**,
429 (2022).

430 9. Falhof, J., Pedersen, J. T., Fuglsang, A. T. & Palmgren, M. Plasma Membrane H+-
431 ATPase Regulation in the Center of Plant Physiology. *Mol. Plant* **9**, 323–337 (2016).
432 10. Meng, X. & Zhang, S. MAPK cascades in plant disease resistance signaling. *Annu. Rev.*
433 *Phytopathol.* **51**, 245–266 (2013).
434 11. Harwood, C. R., Mouillon, J.-M. M., Pohl, S. & Arnau, J. Secondary metabolite
435 production and the safety of industrially important members of the Bacillus subtilis
436 group. *FEMS Microbiol. Rev.* **42**, 721–738 (2018).
437 12. Cawoy, H. *et al.* Plant Defense Stimulation by Natural Isolates of *Bacillus* Depends on
438 Efficient Surfactin Production. *Mol. Plant-Microbe Interact.* **27**, 87–100 (2014).
439 13. Torres, M. A., Dangl, J. L. & Jones, J. D. G. Arabidopsis gp91phox homologues Atrbohd
440 and Atrbohf are required for accumulation of reactive oxygen intermediates in the
441 plant defense response. *Proc. Natl. Acad. Sci. U. S. A.* **99**, 517–522 (2002).
442 14. Morales, J., Kadota, Y., Zipfel, C., Molina, A. & Torres, M. A. The Arabidopsis NADPH
443 oxidases RbohD and RbohF display differential expression patterns and contributions
444 during plant immunity. *J. Exp. Bot.* **67**, 1663–1676 (2016).
445 15. Shang-Guan, K. *et al.* Lipopolysaccharides trigger two successive bursts of reactive
446 oxygen species at distinct cellular locations. *Plant Physiol.* **176**, 2543–2556 (2018).
447 16. Arnaud, D., Deeks, M. J. & Smirnoff, N. Organelle-targeted biosensors reveal distinct
448 oxidative events during pattern-triggered immune responses. *Plant Physiol.* **191**,
449 2551–2569 (2022).
450 17. Ashtamker, C., Kiss, V., Sagi, M., Davydov, O. & Fluhr, R. Diverse subcellular locations
451 of cryptogein-induced reactive oxygen species production in tobacco bright yellow-2
452 cells. *Plant Physiol.* **143**, 1817–1826 (2007).
453 18. Stringlis, I. A. *et al.* Root transcriptional dynamics induced by beneficial rhizobacteria

454 and microbial immune elicitors reveal signatures of adaptation to mutualists. *Plant J.*
455 **93**, 166–180 (2018).
456 19. Bjornson, M., Pimprikar, P., Nürnberger, T. & Zipfel, C. The transcriptional landscape
457 of Arabidopsis thaliana pattern-triggered immunity. *Nat. Plants* **7**, 579–586 (2021).
458 20. Müller, T. M. *et al.* Transcription activator-like effector nuclease-mediated generation
459 and metabolic analysis of camalexin-deficient cyp71a12 cyp71a13 double knockout
460 lines. *Plant Physiol.* **168**, 849–858 (2015).
461 21. Ferrari, S., Plotnikova, J. M., De Lorenzo, G. & Ausubel, F. M. Arabidopsis local
462 resistance to Botrytis cinerea involves salicylic acid and camalexin and requires EDS4
463 and PAD2, but not SID2, EDS5 or PAD4. *Plant J.* **35**, 193–205 (2003).
464 22. Denoux, C. *et al.* Activation of defense response pathways by OGs and Flg22 elicitors
465 in Arabidopsis seedlings. *Mol. Plant* **1**, 423–445 (2008).
466 23. Glazebrook, J. & Ausubel, F. M. Isolation of phytoalexin-deficient mutants of
467 Arabidopsis thaliana and characterization of their interactions with bacterial
468 pathogens. *Proc. Natl. Acad. Sci. U. S. A.* **91**, 8955–8959 (1994).
469 24. Kutschera, A. *et al.* Bacterial medium-chain 3-hydroxy fatty acid metabolites trigger
470 immunity in Arabidopsis plants. *Science (80-.).* **364**, 178–181 (2019).
471 25. Schellenberger, R. *et al.* Bacterial rhamnolipids and their 3-hydroxyalkanoate
472 precursors activate Arabidopsis innate immunity through two independent
473 mechanisms. *Proc. Natl. Acad. Sci. U. S. A.* **118**, 1–10 (2021).
474 26. Liang, X. & Zhou, J. M. Receptor-Like Cytoplasmic Kinases: Central Players in Plant
475 Receptor Kinase-Mediated Signaling. *Annu. Rev. Plant Biol.* **69**, 267–299 (2018).
476 27. Albert, I. *et al.* An RLP23–SOBIR1–BAK1 complex mediates NLP-triggered immunity.
477 *Nat. Plants* **1**, 15140 (2015).

478 28. Fan, L. *et al.* Genotyping-by-sequencing-based identification of Arabidopsis pattern
479 recognition receptor RLP32 recognizing proteobacterial translation initiation factor
480 IF1. *Nat. Commun.* **13**, (2022).
481 29. Wan, W. L. *et al.* Comparing Arabidopsis receptor kinase and receptor protein-
482 mediated immune signaling reveals BIK1-dependent differences. *New Phytol.* **221**,
483 2080–2095 (2019).
484 30. Henry, G., Deleu, M., Jourdan, E., Thonart, P. & Ongena, M. The bacterial lipopeptide
485 surfactin targets the lipid fraction of the plant plasma membrane to trigger immune-
486 related defence responses. *Cell. Microbiol.* **13**, 1824–1837 (2011).
487 31. Balleza, D., Alessandrini, A. & Beltrán García, M. J. Role of Lipid Composition,
488 Physicochemical Interactions, and Membrane Mechanics in the Molecular Actions of
489 Microbial Cyclic Lipopeptides. *J. Membr. Biol.* **252**, 131–157 (2019).
490 32. Rondelli, V. *et al.* Sitosterol and glucosylceramide cooperative transversal and lateral
491 uneven distribution in plant membranes. *Sci. Rep.* **11**, 1–11 (2021).
492 33. Gronnier, J., Gerbeau-Pissot, P., Germain, V., Mongrand, S. & Simon-Plas, F. Divide
493 and Rule: Plant Plasma Membrane Organization. *Trends Plant Sci.* **23**, 899–917 (2018).
494 34. Haslam, T. M. & Feussner, I. Diversity in sphingolipid metabolism across land plants. *J.*
495 *Exp. Bot.* **73**, 2785–2798 (2022).
496 35. Ternes, P. *et al.* Disruption of the ceramide synthase LOH1 causes spontaneous cell
497 death in Arabidopsis thaliana. *New Phytol.* **192**, 841–854 (2011).
498 36. Lenarčič, T. *et al.* Eudicot plant-specific sphingolipids determine host selectivity of
499 microbial NLP cytolysins. *Science (80-.).* **358**, 1431–1434 (2017).
500 37. Gerbeau-Pissot, P. *et al.* Modification of plasma membrane organization in tobacco
501 cells elicited by cryptogein. *Plant Physiol.* **164**, 273–286 (2014).

502 38. Sandor, R. *et al.* Plasma membrane order and fluidity are diversely triggered by
503 elicitors of plant defence. *J. Exp. Bot.* **67**, 5173–5185 (2016).
504 39. McKenna, J. F. *et al.* The cell wall regulates dynamics and size of plasma-membrane
505 nanodomains in Arabidopsis. *Proc. Natl. Acad. Sci. U. S. A.* **116**, 12857–12862 (2019).
506 40. Vaahtera, L., Schulz, J. & Hamann, T. Cell wall integrity maintenance during plant
507 development and interaction with the environment. *Nat. Plants* **5**, 924–932 (2019).
508 41. Basu, D. & Haswell, E. S. The Mechanosensitive Ion Channel MSL10 Potentiates
509 Responses to Cell Swelling in Arabidopsis Seedlings. *Curr. Biol.* **30**, 2716-2728.e6
510 (2020).
511 42. Martinac, B., Adler, J. & Kung, C. Mechanosensitive ion channels of E. coli activated by
512 amphipaths. *Nature* **348**, 261–263 (1990).
513 43. Hamilton, E. S., Schlegel, A. M. & Haswell, E. S. United in Diversity: Mechanosensitive
514 Ion Channels in Plants. *Annu. Rev. Plant Biol.* **66**, 113–137 (2014).
515 44. Hamant, O. & Haswell, E. S. Life behind the wall: Sensing mechanical cues in plants.
516 *BMC Biol.* **15**, 1–9 (2017).
517 45. Demidchik, V., Shabala, S., Isayenkov, S., Cuin, T. A. & Pottosin, I. Calcium transport
518 across plant membranes: mechanisms and functions. *New Phytol.* **220**, 49–69 (2018).
519 46. Yoshimura, K., Iida, K. & Iida, H. MCAs in Arabidopsis are Ca2+-permeable
520 mechanosensitive channels inherently sensitive to membrane tension. *Nat. Commun.*
521 **12**, 6074 (2021).
522 47. Thor, K. *et al.* The calcium-permeable channel OSCA1.3 regulates plant stomatal
523 immunity. *Nature* **585**, 569–573 (2020).
524 48. Haswell, E. S., Peyronnet, R., Barbier-Brygoo, H., Meyerowitz, E. M. & Frachisse, J. M.
525 Two MscS Homologs Provide Mechanosensitive Channel Activities in the Arabidopsis

526 Root. *Curr. Biol.* **18**, 730–734 (2008).

527 49. Yamanaka, T. *et al.* MCA1 and MCA2 That Mediate Ca2+ Uptake Have Distinct and
528 Overlapping Roles in Arabidopsis. *Plant Physiol.* **152**, 1284–1296 (2010).

529 50. Mori, K. *et al.* Ca2+-permeable mechanosensitive channels MCA1 and MCA2 mediate
530 cold-induced cytosolic Ca2+ increase and cold tolerance in Arabidopsis. *Sci. Rep.* **8**,
531 550 (2018).

532 51. Moe-Lange, J. *et al.* Interdependence of a mechanosensitive anion channel and
533 glutamate receptors in distal wound signaling. *Sci. Adv.* **7**, (2021).

534 52. Schellenberger, R. *et al.* Bacterial rhamnolipids and their 3-hydroxyalkanoate
535 precursors activate Arabidopsis innate immunity through two independent
536 mechanisms. *Proc. Natl. Acad. Sci. U. S. A.* **118**, 2101366118 (2021).

537 53. Schellenberger, R. *et al.* Apoplastic invasion patterns triggering plant immunity:
538 plasma membrane sensing at the frontline. *Mol. Plant Pathol.* **20**, 1602–1616 (2019).

539 54. Schikora, A., Schenk, S. T. & Hartmann, A. Beneficial effects of bacteria-plant
540 communication based on quorum sensing molecules of the N-acyl homoserine lactone
541 group. *Plant Mol. Biol.* **90**, 605–612 (2016).

542 55. Davis, B. M., Jensen, R., Williams, P. & O'Shea, P. The Interaction of N-Acylhomoserine
543 Lactone Quorum Sensing Signaling Molecules with Biological Membranes:
544 Implications for Inter-Kingdom Signaling. *PLoS One* **5**, e13522 (2010).

545 56. Girard, L., Höfte, M. & Mot, R. De. Lipopeptide families at the interface between
546 pathogenic and beneficial Pseudomonas-plant interactions. *Critical Reviews in*
547 *Microbiology* **46**, 397–419 (2020).

548 57. Jin, M. S. *et al.* Crystal Structure of the TLR1-TLR2 Heterodimer Induced by Binding of
549 a Tri-Acylated Lipopeptide. *Cell* **130**, 1071–1082 (2007).

550 58. Debois, D. *et al.* Plant polysaccharides initiate underground crosstalk with bacilli by
551 inducing synthesis of the immunogenic lipopeptide surfactin. *Environ. Microbiol. Rep.*
552 **7**, 570–582 (2015).
553 59. He, Z., Webster, S. & He, S. Y. Growth–defense trade-offs in plants. *Current Biology* **32**,
554 R634–R639 (2022).
555

Figure 1

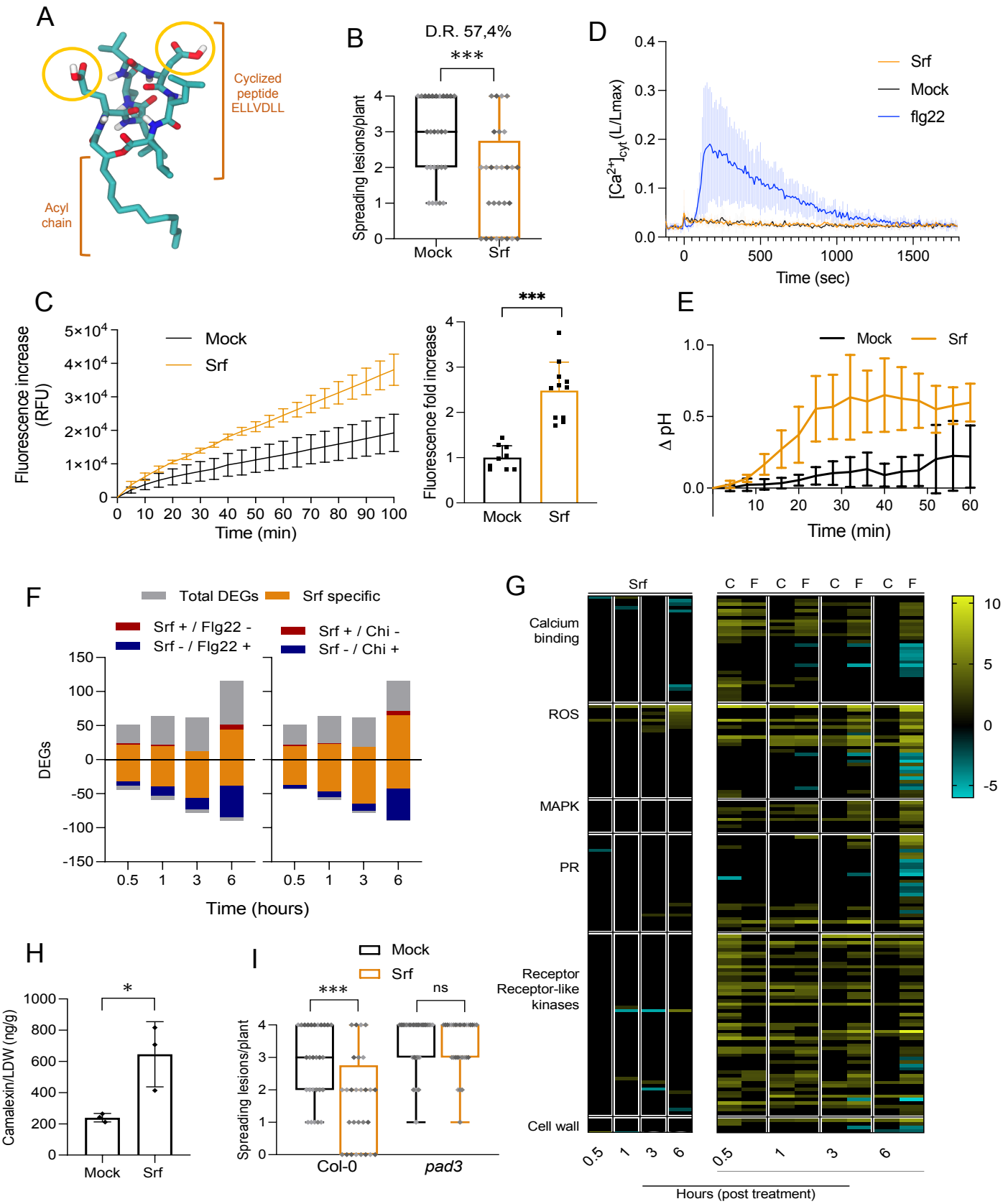
A
Cyclized peptide ELLVDLL
Acyl chain
B
D.R. 57,4%
***
Spreading lesions/plant
Mock
Srf
D
Srf
Mock
flg22
[Ca2+]cyt (L/Lmax)
Time (sec)
C
Mock
Srf
Fluorescence increase (RFU)
Time (min)
***
Fluorescence fold increase
Mock
Srf
E
Mock
Srf
Δ pH
Time (min)
F
Total DEGs
Srf specific
Srf + / Flg22 -
Srf - / Flg22 +
Srf + / Chi -
Srf - / Chi +
DEGs
Time (hours)
G
Srf
C F C F C F C F
Calcium binding
ROS
MAPK
PR
Receptor Receptor-like kinases
Cell wall
Hours (post treatment)
H
*
Camalexin/LDW (ng/g)
Mock
Srf
I
Mock
Srf
***
ns
Spreading lesions/plant
Col-0
pad3

Figure 2

A

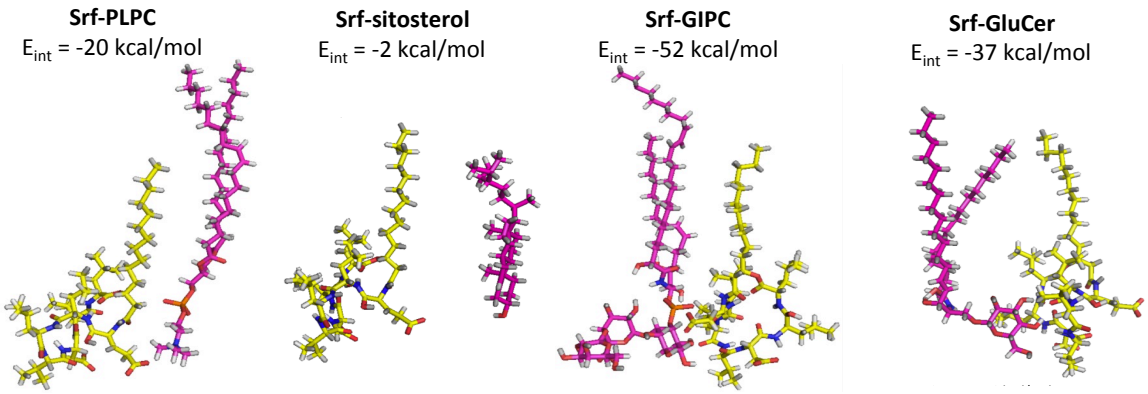

B

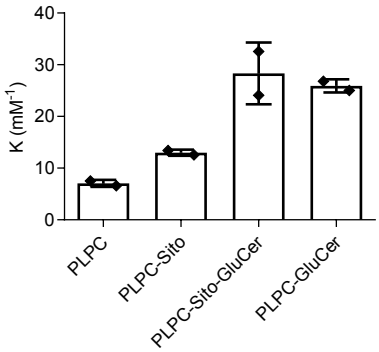

C

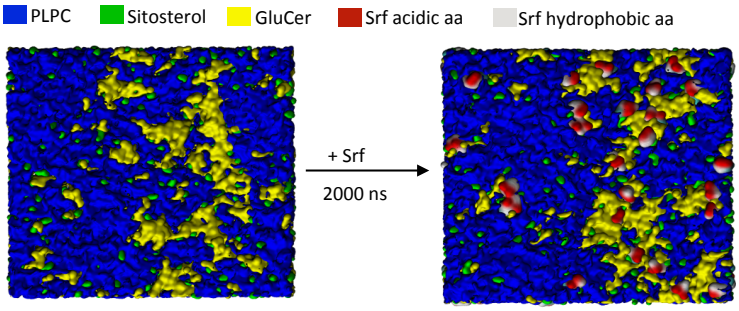

D

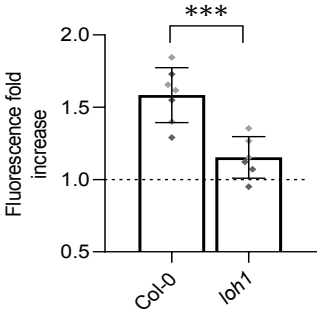

E

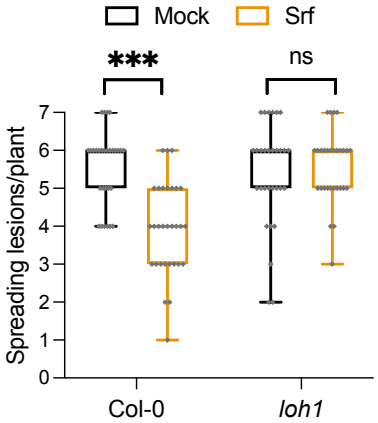

Figure 3

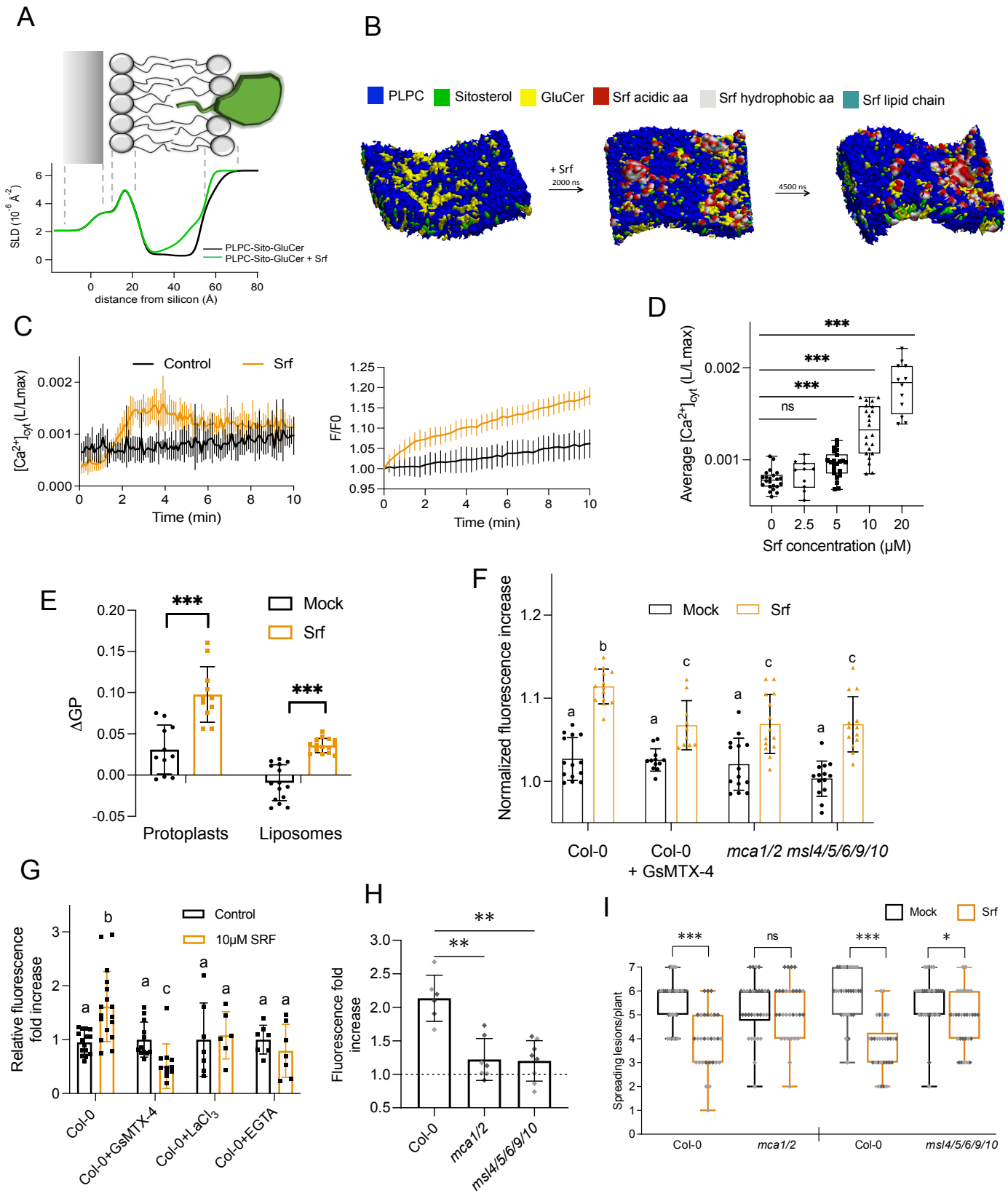
A
SLD (10^{-6} Å^{-2})
PLPC-Sito-GluCer
PLPC-Sito-GluCer + Srf
distance from silicon (Å)
B
PLPC
Sitosterol
GluCer
Srf acidic aa
Srf hydrophobic aa
Srf lipid chain
+ Srf
2000 ns
4500 ns
C
Control
Srf
$[Ca^{2+}]_{cyt}$ (L/Lmax)
Time (min)
F/F0
Time (min)
D
Average $[Ca^{2+}]_{cyt}$ (L/Lmax)
Srf concentration (µM)
E
Mock
Srf
ΔGP
Protoplasts
Liposomes
F
Mock
Srf
Normalized fluorescence increase
Col-0
Col-0 + GsMTX-4
mca1/2 msl4/5/6/9/10
G
Control
10µM SRF
Relative fluorescence fold increase
Col-0
Col-0+GsMTX-4
Col-0+LaCl3
Col-0+EGTA
H
Fluorescence fold increase
Col-0
mca1/2
msl4/5/6/9/10
I
Mock
Srf
Spreading lesions/plant
Col-0
mca1/2
Col-0
msl4/5/6/9/10